10-2014

The Structure-Function Relationship of PAMAM Dendrimers as Robust Oil Dispersants

Nicholas K. Geitner
Clemson University

Bo Wang
Clemson University

Rachel E. Andorfer
Clemson University

David A. Ladner
Clemson University, ladner@clemson.edu

Pu Chen Ke
Clemson University

See next page for additional authors

The Structure-Function Relationship of PAMAM Dendrimers as Robust Oil Dispersants

Nicholas K Geitner,[†] Bo Wang,[†] Rachel E Andorfer,[†] David A Ladner,[‡] Pu Chun Ke,[†] and Feng Ding[†*]

Author Addresses

† Department of Physics and Astronomy, Clemson University, Clemson, SC 29634, USA

‡ Department of Environmental Engineering and Earth Sciences, Clemson University, Clemson, SC 29634, USA

*Corresponding Author. E-mail: fding@clemson.edu

ABSTRACT

PAMAM dendrimers have recently been investigated as efficient and biocompatible oil dispersants utilizing their encapsulation capacity; however, their high cationic charge density has been shown to be cytotoxic. It is therefore imperative to mitigate cationic charge-induced toxicity and understand the effects of such changes. Presented here is a synergistic experimental and computational approach to examine the effects of varying terminal surface charge on the capacity of dendrimers to disperse model liner, polycyclic aromatic, and hybrid hydrocarbons. Uncharged dendrimers collapse by forming intra-molecular hydrogen bonds, which reduce the hosting capability. On the other hand, changing the surface charges from positive to negative greatly shifts the pKa of tertiary amines of the PAMAM dendrimer interior. As a result, the negatively charged dendrimers have a significant percentage of tertiary amines protonated, ~30%. This unexpected change in interior protonation state cause electrostatic interactions with the anionic terminal groups, leading to contraction and a marked decrease in hydrocarbon hosting capacity. The present work highlights the robust nature of dendrimer oil dispersion and

also illuminates potentially unintended or unanticipated effects of varying dendrimer surface chemistry on their encapsulation or hosting efficacy, which is important for their environmental, industrial, and biomedical applications.

1. INTRODUCTION

Originally proposed by Paul Flory,[1] dendritic polymers are a class of macromolecules consisting of highly branched polymer units. Within this class are dendrons, dendrimers, and hyperbranched polymers.[1] Dendrimers can be precisely synthesized with high order and monodispersion, with well defined branching units emanating from a central core.[1] The number of these branching iterations is termed the Generation of the dendrimer and determines its size, structure, and function. Hyperbranched polymers, in contrast, possess less well-defined branched interiors, resulting in a higher polydispersity at a much lower production cost. Due to their unique physicochemical properties, there are a wide variety of current and potential applications of dendrimers ranging from environment to energy and biomedicine. For example, hydroxyl-terminated PAMAM dendrimers have been shown to remove contaminants such as humic acids[2] and metal ions[3,4] from drinking water or contaminated soils. Dendrimers can be used in light-harvesting applications for superior transduction efficiency in diodes and other photonic devices.[5,6] The surface functionality of PAMAM dendrimers has been altered to include long-lifetime ibuprofen release *in vivo*[7] and conjugation with partially anionic folate-conjugates has been explored for the delivery of anti-arthritic drugs.[8] The ability of dendrimers to encapsulate small organic molecules has also been studied in terms of dendrimer generation[9] as well as the shape of a guest molecule,[10] demonstrating a wide array of hosting capabilities of dendrimers in aqueous solution.

Given their hosting capabilities, we have previously proposed PAMAM polymers as oil dispersants,[11] and showed that cationic PAMAM dendrimers are capable of hosting both polyaromatic and linear hydrocarbons in water.[11] Conventionally, lipid-like oil dispersants have been in use since at least the 1960s[12] and also during the large scale Deepwater Horizon disaster of 2010. However, concerns over the potential toxicity of conventional oil dispersants have been recently raised.[13–15] There is a renewed and pressing desire for effective yet biocompatible dispersing agents. Our previous work has shown, however, that highly cationic amine-terminated poly(amidoamine) (PAMAM) dendrimers cause acute toxicity in amoebas at a high concentration.[16] Similarly, several other studies have also shown that highly cationic PAMAM dendrimers cause significant charge-induced toxicity *in vitro*[17–20] and rapid blood clotting *in vivo*.[21] It has been suggested that the electrostatic interaction between highly cationic PAMAM and negatively charged cell membrane results in pore formation to trigger cytotoxicity. Therefore, efforts are increasingly being focused on altering dendrimer terminal charges in order to reduce the toxicity or improve the efficacy of dendrimer agents.[22,23]

Many studies have been conducted on the size, structure, and dynamics of dendrimers depending on dendrimer generation[24,25] and environmental conditions such as solution pH and ionic strength.[24–28] It has been shown that PAMAM dendrimers adopt globular-like structures with the repeating monomers loosely packed in the interior and the surface groups protruding, forming hydrogen bonds with water. Simulations revealed dynamically forming pores in the interior that can bind various guest molecules.[24,29] Solution pH and ionic strength can also affect dendrimer structure by changing the dendrimer protonation states and screening of electrostatic interactions, respectively.[26,27,30] It is not understood, however, how surface modifications of

dendrimers, a common strategy in dendrimer design and synthesis, might affect their size, structure, dynamics, and subsequent functionality.

Here, we investigate the effects of varying the surface charge and functionality on dendrimers' ability to serve as effective oil dispersants. Specifically, we examine cationic amine-terminated (G4-NH_2), neutral hydroxyl-terminated (G4-OH), and anionic succinamic acid-terminated (G4-SA) PAMAM dendrimers (Fig. 1A). Synergistic experiments and molecular dynamics simulations are performed to probe the interactions, limitations, mechanisms, and differences between cationic, anionic, and neutrally charged PAMAM dendrimers with linear, polyaromatic, and hybrid hydrocarbons as well as the combination thereof. These various combinations of hydrocarbon are studied in order to gain a more fundamental understanding of dendrimer oil dispersant interactions with the various hydrocarbon components of crude oil as well as illuminate any potential synergistic dispersion effects of hydrocarbon mixtures. The advantages of model hydrocarbons over whole crude oil include the real-time tracking and accurate quantification for mechanistic studies of the structure-function relationship. Additional studies of dendrimer dispersion efficacy and toxicity with crude oil have been done in a separate work. The implications of this study reach beyond oil dispersion to other biomedical and environmental applications including drug delivery and water purification, noting the differences in dendrimer interactions with aliphatic and aromatic hydrophobic molecules as well as potentially unanticipated effects of altering dendrimer surface functionality. We find that marked differences in hosting capacity for hydrocarbons arise from changes in both the structure and dynamics of the dendrimers with varying terminal functionality.

2. EXPERIMENTAL

2.1 Materials and Characterization. All dendrimers were purchased from Dendritech, Inc. and were PAMAM G4.0 (generation four) in water solvent and stored at 4°C. Phenanthrene (PN) and octadecylbenzene (ODB) were purchased from Sigma-Aldrich, hexadecane (C_{16}) from Acros Organics and all stored at room temperature. The dendrimer stock solutions were diluted in DI water (18 MΩ cm) to a final concentration of 15 µM, and their pH adjusted to 8.2 to mimic that of seawater using 1M NaOH and 1M HCl. Dynamic light scattering (DLS) and zeta potential characterizations of these prepared stock solutions were carried out on a NanoBrook ZetaPALS.

2.2 UV-vis Spectophotometry and Phenanthrene Affinity. UV-vis spectroscopy absorbance measurements were performed on a temperature-controlled Cary 300 Bio (Thermo Electric Corp.). To normalize the concentration of PN, a known quantity was dissolved in methanol and the intensity of the absorbance peak at 251 nm was measured. This relation was then used to calculate all other PN concentrations. The concentration of dendrimer-associated PN was calculated using Eqn. (1) where $[PN]_T$ is the total observed concentration of PN in the column and $[PN]_S$ is the concentration of free PN in solution.

$$[D \cdot PN]=[PN]_T-[PN]_S \quad (1)$$

A solution of 15 µM dendrimers was used as a control in all measurements of PN with dendrimers. Each sample was prepared with 1 mg of PN added to 2 mL of either water or dendrimer stock solution. Samples were bath sonicated for 5 min (Branson) in order to break PN solids and then rotated overnight to reach equilibrium. We then measured the affinity of dendrimers for PN in water as a function of temperature by measuring the absorbance of PN over a temperature range from 20-80ºC. The temperature was increased at a rate of 0.1ºC/min, and absorbance was measured every 1.0 ± 0.02ºC. These measurements were made in triplicate in

sealed quartz cuvettes. The apparent association constant K was calculated using Eqn. (2) where [D] is the free dendrimer concentration.

$$K=[D\cdot PN]/([D][PN]_S) \quad (2)$$

Solutions of PN dissolved in C_{16} were prepared such that the final solution was 8% PN by weight dissolved in C_{16}. For sample incubations, 20 µL of this stock was added to 2 mL of either water or dendrimer solution and then rotated for 1 h. This ensured that the same total mass of PN was added as in the pure PN experiments. The same temperature ramp as above was then performed, again by measuring the absorbance of PN at 251 nm.

2.3 Fluorescence. Fluorescence measurements were performed on a temperature-controlled Cary Eclipse fluorometer (Thermo Electric Corp.). ODB-doped C_{16} stock was prepared such that the hydrocarbon solution was 2.6% ODB by weight. For all measurements with ODB, 65 µL of stock solution was added to 2 mL of water or dendrimer solution and then rotated gently for 1 h. It was then allowed to settle, and solution was pulled from the middle of each tube to avoid phase-separated oil. Then 20 µL of stock ODB-doped C_{16} was added to each cuvette to ensure a consistent excess of available hydrocarbons. The fluorescence emission was observed at both wavelengths of 290 nm and 299 nm, with an excitation wavelength of 258 nm in both cases. The fluorescence emission intensities were recorded every 1.0 ± 0.02ºC in the same temperature ramp as described in Section 2.2.

2.4 DMD Simulations. Discrete molecular dynamics (DMD) is a special type of molecular dynamics algorithm, featuring rapid dynamics sampling efficiency. The detailed algorithm and force field parameterization of DMD can be found elsewhere.[31] We used a united atom

representation to model the molecular system, explicitly modeling all polar hydrogen and heavy atoms and with implicit solvent. Inter-atomic interactions were modeled by a physical force field adapted from Medusa,[32,33] which included Van der Waals (VDW), solvation, electrostatic and hydrogen bond interactions. The force field parameters for VDW interactions, bond length, angle and dihedral angles were taken from CHARMM 19. The solvation energy was included using the Lazaridis-Karplus implicit solvent model. The distance and angular dependant hydrogen bond interaction was modeled using a reaction-like algorithm.[32] We used the Debye-Hückel approximation to model the screened electrostatic interactions between charged atoms. The Debye length was approximately 10 Å by assuming water relative permittivity of 80, and a monovalent electrolyte concentration of 0.1 mM.

The starting structures of dendrimers were generated by constructing the idealized 3-dimensional dendrimer structure consisting of a core, branching units, and terminal groups, followed by equilibration and energy minimization. To emulate a solution pH of 8.2, all G4-NH_2 and G4-SA terminal groups were charged (protonated and deprotonated, respectively). All tertiary amines in G4-NH_2 and G4-OH were deprotonated and therefore uncharged. To model the partial protonation of tertiary amines in the presence of acid terminal groups, the protonation state of the interior tertiary amines of G4-SA was varied, where 0, 10, 20, or 30% of randomly selected tertiary amines were protonated. In our simulations, the net charges of the molecular systems were maintained zero by adding offsetting charges, such as chloride (Cl^-) and sodium (Na^+) ions. After the initialization of dendrimer structures, energy minimization using DMD was carried out for 10,000 time steps (approximately 10 ns) before carrying out further equilibrium simulations.

In DMD simulations, temperature is in the unit of kcals/mol·k_B, where k_B is the Boltzmann constant. Our simulations were conducted for a temperature range of 0.55-0.75 kcal/mol·k_B, corresponding approximately to 275-375 K. The Anderson's thermostat[34] was used to perform constant temperature simulations. At each temperature, energy minimization was first carried out for 10 ns and the simulations were conducted for 2 million time steps (approximately 1 μs), corresponding to an average of approximately 72 CPU hours. We characterized the sizes of all three types of dendrimers by measuring the radius of gyration (R_g) as a function of temperature. The mean and standard deviation of R_g were obtained from 8,000 snapshots evenly distributed throughout the final 800 ns of simulation.

3. RESULTS AND DISCUSSION

Distinctive Physicochemical Properties of Dendrimers with Modified Terminal Groups. Generation 4 PAMAM dendrimers of positively (NH_2), negatively (SA), and neutrally (OH) charged functional groups, all at pH 8.2, were first incubated with PN. We measured the concentration of saturated PN in water and in dendrimer solution with an excess of PN (see Eqn. (1), section 2.2 in Methods; Fig. S1), and computed the concentration of dendrimer-associated PN [D·PN]. We determined the [D·PN], quantifying the capacity of dendrimer to host PN, as a function of temperature (Fig. 1a). The temperature range of 20-80 ºC was chosen to examine the fundamental differences in dendrimer behavior and interactions with hydrocarbons at environmentally relevant temperatures and beyond. Initially, the positively and negatively charged dendrimers have similar hosting capacities, while the neutrally charged dendrimer has lower hosting capacity. As temperature increases in all cases there is an increased hosting of PN by dendrimers, in part due to the increasing availability of PN in solution with increasing

temperature. This trend continues until approximately 74ºC for positively and neutrally charged dendrimers, at which point the PN hosting capacity reaches a peak followed by a marked decrease. In contrast, negatively charged dendrimers reach their maximum capacity between 65-74ºC, reaching just 56% the maximum PN hosting of G4-NH_2.

With the measured PN concentrations in water and in dendrimers as well as the concentration of dendrimers in solution, we can calculate the apparent association constants, K (see Eqn. (2), Section 2.2 in Methods) and compute logK as a function of temperature (Fig. 1b). For NH_2 and SA-terminated dendrimers, we observe relatively constant, large apparent association constants at low temperatures. In contrast, the neutral OH-terminated dendrimers had a much lower affinity at low temperature, but this affinity surprisingly increases rapidly with respect to increased temperature and becomes nearly identical to the NH_2-terminated affinity near 70ºC. Both G4-NH_2 and G4-OH dendrimer affinity for PN sharply drop at 74ºC, as expected (see Fig. 1a). Despite the more significant and gradual decrease in G4-SA affinity, we note an increase in this rate of decrease at the same 74ºC, indicating the temperature at which it becomes thermodynamically more favorable for PN to dissolve in water than to be partitioned inside of the dendrimers, as PN water solubility increases exponentially with temperature over the observed range (Figure S1). Therefore, the changes in dendrimer surface charge result in drastic changes in its hosting capacity of PN and the temperature dependences. However, since PN is non-charged and the binding is not governed by electrostatic interactions, it is intriguing as what the molecular mechanism is for such drastic changes in hydrocarbon hosting capacity upon adjusting the dendrimer surface charges.

We postulated that the changes are mostly in the structure of dendrimer, which in turn affect the hosting function of dendrimer. We first characterized the size and charge properties of

all three types of dendrimers in solution (Table 1) using DLS and PALS zeta potential measurements, respectively (Methods). The DLS results suggest that the dendrimers are fairly monodisperse and tend not to aggregate in DI water. Second, that the OH-terminated dendrimers have smaller hydrodynamic diameters (D_H) than their charged counterparts. The zeta (ζ) potential quantifies the dendrimer net electrokinetic potential in solution. We find that, indeed, the OH-terminated dendrimers carry nearly zero net charge and the amine-terminated dendrimers are highly positively charged (+30 mV). Interestingly, the SA-terminated, while negatively charged, carry a net charge with significantly smaller magnitude than the amine-terminated. This reduction of overall net charge suggests that some of the interior tertiary amines in SA-terminated dendrimers may become protonated at this pH. Assuming electric multilayers similar in nature, the measured differences in zeta potential magnitude suggest the protonation of approximately 30% of G4-SA tertiary amines. Such a significant shift in pKa of the tertiary amine compared to neutral and positively charged dendrimers is feasible in the presence of a large number of terminal acidic groups in the vicinity.[35] These characterizations suggest significant physicochemical differences in PAMAM dendrimers caused simply by varying the terminal functionality. Next, we perform molecular dynamics simulations to study the changes of dendrimer size and structure with respect to surface charges at the molecular level.

We performed DMD simulations of all three dendrimer classes (Methods) and measured the radius of gyration (R_g) as a function of temperature (Fig. 2a) for each case. For the SA-terminated dendrimers, we studied the effect of partial protonation of their tertiary amines, with levels of protonation ranging from 0-30% protonation, where 30% tertiary protonation corresponds to the experimentally observed zeta potential of G4-SA. In DMD simulations, the dendrimer rapidly reaches equilibrium with *Rg* fluctuating around its average value in a long

timescale simulation trajectory (~50 ns; Figure S2). Across the simulated temperature range, the R_g of G4-NH_2 increases from 19.4 Å to 21.25 Å, in agreement with small angle neutron scattering (SANS) experiments as well as atomistic molecular dynamics (MD) and coarse-grained (CG) simulations performed elsewhere (Table 2, Fig. S3).[36–40] Because R_g is an averaged single-value measurement, we also calculate the radial density function (RDF) to quantify the internal structure of dendrimers (Figs. S4 & S5). As observed previously in an all-atom MD simulations[41], we find that lower generations exhibit denser core structures while higher generations G4-G5 are more open due to increased electrostatic repulsion between terminal groups (Fig. S4). We also computed the RDF for the G4-NH_2 dendrimers at different pH values. At high pH, the primary amines are fully depronated, making the dendrimer neutrally charged. At low pH, the tertiary amines are protonated and the dendrimer is fully charged. Our results confirm the expected transition from dense-core at high pH to dense-shell configuration at neutral and low pH as observed in previous all-tom MD simulations (Fig. S5).[39] This validates our DMD-derived simulations as efficient and robust for studies of dendrimer structure and dynamics. G4-SA is, across the simulated temperature range, larger than G4-NH_2 due to the slightly longer terminal groups. Their R_g values decrease with increasing tertiary amine protonation, and at the lowest tested temperature it reduces from approximately 22.25 Å at 0% protonation to just 20.0 Å once 30% of the interior tertiary amines have been protonated. This size change is because of the electrostatic attraction between these protonated groups and the negatively charged terminal carboxyl groups. This attraction also limits the expansion of G4-SA with temperature: e.g. G4-SA(30%) swells just 1.25 Å compared to a 1.9 Å growth seen in G4-NH_2, resulting in equal R_g values at the highest temperature in simulations.

While amine- and SA-terminated dendrimers have similar sizes across the entire temperature range, G4-OH is clearly smaller than its charged counterparts, expanding from an R_g of 16.25 to 18.13 Å at the lowest and highest simulation temperatures, respectively. This markedly smaller size is due to the lack of electrostatic repulsion between terminal groups and hydrogen bond formation between the terminal hydroxyl groups, resulting in a much more compact dendrimer structure (e.g. typical snapshot structures in Fig. 2b).

These differences in size and how sizes change with temperature in simulations is consistent with the experimentally observed differences in apparent affinity for PN as in Fig. 1. G4-OH has a much lower affinity for PN at low temperatures because, at those temperatures, they are significantly more compact than either G4-SA or -NH_2, thus reducing the size and accessibility of the interior voids to host PN as illustrated by the dense-core structure of the neutrally charged dendrimer (Fig. S4). As temperature increases, the G4-OH expands with increased R_g by breaking the hydrogen bonds, thereby granting access to its growing interior cavities. Our zeta-potential characterization of G4-NH_2 and G4-SA suggests that approximately 30% of the G4-SA tertiary amines are protonated (Fig. 2c) assuming tertiary amines in G4-NH_2 are not protonated.[22] This change allows strong electrostatic interaction between terminal groups and the protonated tertiary amines, which causes the dendrimer to contract relative to the less protonated G4-SA dendrimers. Such strong electrostatic interaction also noticeably inhibits size expansion with temperature in contrast to the weaker hydrogen bond interaction in G4-OH (Fig. 2a). As a result, the G4-SA features a lower host capacity and apparent affinities for PN compared to G4-NH_2. These differences in swelling behavior highlight why the temperature dependence in PN hosting capacity is different for each dendrimer despite all three functionalizations growing with increasing temperature. Such a dependence on hydrophobic core

accessible for hosting small hydrophobic molecules is in agreement with earlier studies by Tomalia *et al* with lipophilic dye encapsulation by dendrimers of various generations.[9] In addition, since the dendrimer volume available for hosting increases rapidly as the cubic power of the size, a small change in *Rg* (Fig. 2) leads to large changes in hosting capacity (Fig. 1). It is also important to note that, by charging a fraction of the interior groups, the interior voids become slightly less hydrophobic and thus less favorable for hydrocarbon interactions. Another interesting observation in experiments is the sharp decrease of PN binding at 74ºC for all dendrimers (Fig. 1). We hypothesize that this phenomenon is due to the intrinsic structural properties of dendrimer at different temperatures. As the dendrimers expand with increasing temperature (Fig. 2), the cooperative binding with PN due to interactions among amidoamine monomers is reduced. At high temperatures, the binding is dominated by the interaction between PN and amidoamine monomer. Therefore, the transition at 74ºC is the result of dissociation of PN from amidoamine monomer to the solution.

Hosting of Various Classes of Hydrocarbons and Their Mixtures. Having examined the differences between dendrimers of different surface charge, we are now interested in binding between PAMAM dendrimers, using G4-NH_2 as our model, and different hydrocarbons. Amine-terminated dendrimers were chosen because they exhibited the strongest binding with hydrocarbons across the tested temperature range, and therefore allowed the best characterization of the differences between PAMAM binding with different classes of hydrocarbons. As crude oils are composed largely of aliphatic hydrocarbons, it is critical to understand dendrimer interactions with such linear hydrocarbons. However, purely aliphatic hydrocarbons are difficult to track quantitatively in solution. To overcome this difficulty, we doped solutions of hexadecane

296 with octadecylbenzene (ODB, 2.5 w/w%), which is an 18-carbon chain with the addition of a
297 benzene ring on one end. The result is a solution with minimal change from a purely aliphatic
298 hydrocarbon mixture but which can be monitored in real time in solution using
299 spectrofluorescence measurements (Figure 3). We characterized the excitation and emission of
300 ODB-doped C_{16} in various conditions: dissolved in 100% methanol, suspended as an oil-in-water
301 emulsion in DI water, and in a DI solution of 15 μM G4-NH_2 dendrimers (Fig. 3a). We note that
302 the emission peak redshifts from 281 to 290 nm when suspended in water compared to in
303 methanol, which we attribute to an increased polarity of the fluorophore environment. The ODB
304 emission further redshifts to 299 nm upon incubation with dendrimers, indicating that a
305 significant fraction of ODB molecules interacted directly with G4-NH_2 rather than simply being
306 suspended in smaller droplets of C_{16}. We measured the kinetics of this fluorescence over time,
307 monitoring ODB emissions at 290 and 299 nm for pure water and dendrimer solution samples,
308 respectively (Fig. 3b). While the ODB fluorescence in water and with dendrimers began with
309 nearly identical intensity, there was a marked initial decrease in water-suspended intensity, a loss
310 of approximately 30%. This indicates that many of the emulsion droplets in the water
311 suspensions quickly coalesced before the final stable emulsion was achieved. Even after this
312 relatively stable emulsion was formed, there is a slow (1.4%/h) continued coalescence and a
313 resulting phase separation of the oil-in-water emulsion. Such coalescence is not seen in the
314 dendrimer solution over the observed time period, confirming that such suspensions are more
315 stable than the oil-in-water emulsions. Based on this fluorescence measurement, the stable
316 suspensions formed with G4-NH_2 at room temperature accommodate 57 ± 4% more ODB-doped
317 C_{16} than the oil-in-water emulsion, highlighting the efficiency of dendrimer as oil dispersants.
318 We also note that the nature of the oil dispersion is different from an oil-in-water emulsion

(Inset, Fig. 3b). The oil-in-water emulsion (left) is cloudy due to light scattering by large oil droplets, while the dendrimer-dispersed oil (right) is clear, indicating the presence of much smaller complexes in agreement with previous results that showed the formation of dispersed C_{16}-dendrimer complexes of approximately 200 nm.[11] This further suggests that nearly all suspended hydrocarbons are dendrimer-associated, since we did not observe any oil-in-water droplets that would be expected if dendrimers simply added encapsulated hydrocarbons to an oil-in-water emulsion.

We also examined the fluorescence behavior in water and dendrimer suspensions as a function of temperature (Fig. 3c), showing normalized fluorescence intensities. Note that the initial drop in water suspension fluorescence intensity is due to the coalescence observed at early times as in Fig. 3b, but not due to the increase in temperature. Therefore, normalization for the water curve was performed after this initial drop in intensity. After this point, the water and dendrimer suspensions are statistically identical and both intensities decrease linearly with increasing temperature. This linear decrease in fluorescence intensity with respect to increasing temperature indicates simple thermal quenching as more rotational and vibrational degrees of freedom are accessible with increasing temperature, which is different from the molecular quenching observed between cationic dyes and PAMAM dendrimers with organic moieties.[42] We did not observe any transition as was seen in incubation of pure PN with dendrimers. This is primarily due to the fact that C_{16} has near zero water solubility, therefore eliminating the competition with water solvation seen in the case of PN-dendrimer interactions. Because of this lack of competition, the C_{16}-dendrimer interactions are more stable at high temperatures.

Because crude oil is a combination of aliphatic and aromatic hydrocarbons (among other components), we created a “model crude” by dissolving PN in C_{16} (8% PN) to investigate the

interaction between G4-NH_2 dendrimers and hydrocarbon mixtures. By measuring the UV absorbance of PN as described above, the quantity of oil suspended in the water column with and without dendrimers was calculated (Figure 4). In contrast to the trend seen when incubated with pure PN, the dendrimer-associated PN remains approximately constant with temperature across the entire tested temperature range. These results suggest that the aliphatic C_{16} is able to synergistically facilitate stronger, more stable interactions between dendrimers and PN that have little temperature sensitivity. We hypothesize that C_{16} accomplishes this by eliminating the PN partition competition from water solvation, serving as a stronger solvent inside the dendrimer interior for PN. By assuming that the ratio of PN/C_{16} remains constant after interacting with dendrimers, we calculated the total suspended hydrocarbon concentration. The increase in this total hydrocarbon concentration compared to that in water alone is shown by the shaded area, reaching at least 35 μM hydrocarbon compared to ~10 μM of pure PN (Fig. 1a); the total concentration of hydrocarbons with dendrimers in water reached approximately 135 μM. Because of the behavior noted in the ODB-C_{16} study, we expect that virtually all of the suspended PN and C_{16} were directly dendrimer-associated, which indicates a strong hosting capacity of at least 9 hydrocarbons per dendrimer. This capacity for suspending hydrocarbons persisted well beyond environmentally relevant temperatures, and indeed even beyond the dissociation temperature for pure PN to break down hydrophobic interaction and pi stacking.

In summary, we have shown that aliphatic, aromatic, and hybrid hydrocarbons bind strongly with G4 PAMAM dendrimers at environmentally relevant temperatures. Mixtures of aliphatic and aromatic hydrocarbons in a model crude are synergistically dispersed by PAMAM dendrimers, reaching a highly stable dispersion of at least 9 hydrocarbon molecules per G4 dendrimer over a wide range of temperatures. At environmentally relevant temperatures (*i.e.* less

than approximately 32ºC), G4-SA and G4-NH_2 bind much more strongly to hydrocarbons than G4-OH due to this neutral dendrimer collapsing, closing off access to the hydrophobic interior. However, changes in tertiary amine pKa and resulting interior protonation in G4-SA due to the abundance of terminal acidic groups severely limited their hydrocarbon hosting capacities. The dendrimer oil dispersions were also shown to be significantly more stable and contained 57% more hydrocarbon than simple oil-in-water emulsions. These results demonstrate that, when their versatile physicochemical properties are utilized properly, dendrimers are very robust as oil dispersants; we have also illuminated potentially unanticipated or unintended effects of varying dendrimer surface functionality on hosting applications including dispersion but also drug delivery and water purification that usually deal with hydrophobic or charged ligand species. Future work will include studies examining the effects of pH, ionic strength and ions of different valences in solution.

Acknowledgements

This research was supported in part by US EPA grant RD835182 (to D.L. and F.D.), NSF CBET-1232724 (to P.C.K and F.D.) and Clemson University startup funds (to F.D.). The simulations were performed on the Palmetto high performance cluster, which is managed and maintained by Clemson University CCIT.

References

(1) Tomalia, D. a.; Fréchet, J. M. J. Discovery of Dendrimers and Dendritic Polymers: A Brief Historical Perspective. *J. Polym. Sci. Part A Polym. Chem.* **2002**, *40*, 2719–2728.

(2) Bhattacharya, P.; Conroy, N.; Rao, A. M.; Powell, B. a.; Ladner, D. a.; Ke, P. C. PAMAM Dendrimer for Mitigating Humic Foulant. *RSC Adv.* **2012**, *2*, 7997.

(3) Diallo, M. S.; Balogh, L.; Shafagati, A.; Johnson, J. H.; Goddard, W. A. iii; Tomalia, D. A. Poly (amidoamine) Dendrimers : A New Class of High Capacity Chelating Agents for Cu (II) Ions. *Environ. Sci. Technol.* **1999**, *33*, 820–824.

(4) Xu, Y.; Zhao, D. Removal of Copper from Contaminated Soil by Use of Poly(amidoamine) Dendrimers. *Environ. Sci. Technol.* **2005**, *39*, 2369–2375.

(5) Bradshaw, D. S.; Andrews, D. L. Mechanisms of Light Energy Harvesting in Dendrimers and Hyperbranched Polymers. *Polymers (Basel).* **2011**, *3*, 2053–2077.

(6) Nantalaksakul, A.; Reddy, D. R.; Bardeen, C. J.; Thayumanavan, S. Light Harvesting Dendrimers. *Photosynth. Res.* **2006**, *87*, 133–150.

(7) Kurtoglu, Y. E.; Mishra, M. K.; Kannan, S.; Kannan, R. M. Drug Release Characteristics of PAMAM Dendrimer-Drug Conjugates with Different Linkers. *Int. J. Pharm.* **2010**, *384*, 189–194.

(8) Chandrasekar, D.; Sistla, R.; Ahmad, F. J.; Khar, R. K.; Diwan, P. V. The Development of Folate-PAMAM Dendrimer Conjugates for Targeted Delivery of Anti-Arthritic Drugs and Their Pharmacokinetics and Biodistribution in Arthritic Rats. *Biomaterials* **2007**, *28*, 504–512.

(9) Watkins, D. M.; Sayed-sweet, Y.; Klimash, J. W.; Turro, N. J.; Tomalia, D. A. Dendrimers with Hydrophobic Cores and the Formation of Supramolecular Dendrimer - Surfactant Assemblies. *Langmuir* **1997**, *13*, 3136–3141.

(10) Jansen, J. F. G. A.; Meijer, E. W.; de Brabander-van den Berg, E. M. M. The Dendritic Box: Shape-Selective Liberation of Encapsulated Guests. *J. Am. Chem. Soc.* **1995**, *117*, 4417–4418.

(11) Geitner, N. K.; Bhattacharya, P.; Steele, M.; Chen, R.; Ladner, D. A.; Ke, P. C. Understanding Dendritic Polymer–hydrocarbon Interactions for Oil Dispersion. *RSC Adv.* **2012**, *2*, 9371.

(12) Board, C. on E. of O. D. M. *Using Oil Spill Dispersants on the Sea*; National Academy Press: Washington, D.C., 1989; p. 352.

(13) Anderson, S. E.; Franko, J.; Lukomska, E.; Meade, B. J. Potential Immunotoxicological Health Effects Following Exposure to COREXIT 9500A during Cleanup of the Deepwater Horizon Oil Spill. *Science (80-.).* **2011**, *74*, 1419–1430.

(14) Goodbody-Gringley, G.; Wetzel, D. L.; Gillon, D.; Pulster, E.; Miller, A.; Ritchie, K. B. Toxicity of Deepwater Horizon Source Oil and the Chemical Dispersant, Corexit® 9500, to Coral Larvae. *PLoS One* **2013**, *8*, e45574.

(15) Hemmer, M. J.; Barron, M. G.; Greene, R. M. Comparative Toxicity of Eight Oil Dispersants, Louisiana Sweet Crude Oil (LSC), and Chemically Dispersed LSC to Two Aquatic Test Species. *Environ. Toxicol. Chem.* **2011**, *30*, 2244–2252.

(16) Geitner, N. K.; Powell, R. R.; Bruce, T.; Ladner, D. a.; Ke, P. C. Effects of Dendrimer Oil Dispersants on Dictyostelium Discoideum. *RSC Adv.* **2013**, *3*, 25930.

(17) Petit, A.-N.; Debenest, T.; Eullaffroy, P.; Gagné, F. Effects of a Cationic PAMAM Dendrimer on Photosynthesis and ROS Production of Chlamydomonas Reinhardtii. *Nanotoxicology* **2012**, *6*, 315–326.

(18) Cancino, J.; Paino, I. M. M.; Micocci, K. C.; Selistre-de-Araujo, H. S.; Zucolotto, V. In Vitro Nanotoxicity of Single-Walled Carbon Nanotube-Dendrimer Nanocomplexes against Murine Myoblast Cells. *Toxicol. Lett.* **2013**, *219*, 18–25.

(19) Lewis, T.; Ganesan, V. Interactions between Grafted Cationic Dendrimers and Anionic Bilayer Membranes. *J. Phys. Chem. B* **2013**, *117*, 9806–9820.

(20) Thomas, T. P.; Majoros, I.; Kotlyar, A.; Mullen, D.; Holl, M. M. B.; Baker, J. R. Cationic Poly(amidoamine) Dendrimer Induces Lysosomal Apoptotic Pathway at Therapeutically Relevant Concentrations. *Biomacromolecules* **2009**, *10*, 3207–3214.

(21) Jones, C. F.; Campbell, R. A.; Brooks, A. E.; Assemi, S.; Tadjiki, S.; Thiagarajan, G.; Mulcock, C.; Weyrich, A. S.; Brooks, B. D.; Ghandehari, H.; *et al.* Cationic PAMAM Dendrimers Aggressively Initiate Blood Clot Formation. *ACS Nano* **2012**, *6*, 9900–9910.

(22) Bhattacharya, P.; Geitner, N. K.; Sarupria, S.; Ke, P. C. Exploiting the Physicochemical Properties of Dendritic Polymers for Environmental and Biological Applications. *Phys. Chem. Chem. Phys.* **2013**, *15*, 4477–4490.

(23) Ciolkowski, M.; Petersen, J. F.; Ficker, M.; Janaszewska, A.; Christensen, J. B.; Klajnert, B.; Bryszewska, M. Surface Modification of PAMAM Dendrimer Improves Its Biocompatibility. *Nanomedicine* **2012**, *8*, 815–817.

(24) Maiti, P. K.; Li, Y.; Cagin, T.; Goddard, W. A. Structure of Polyamidoamide Dendrimers up to Limiting Generations: A Mesoscale Description. *J. Chem. Phys.* **2009**, *130*, 144902.

(25) Wu, B.; Kerkeni, B.; Egami, T.; Do, C.; Liu, Y.; Wang, Y.; Porcar, L.; Hong, K.; Smith, S. C.; Liu, E. L.; *et al.* Structured Water in Polyelectrolyte Dendrimers: Understanding Small Angle Neutron Scattering Results through Atomistic Simulation. *J. Chem. Phys.* **2012**, *136*, 144901.

(26) Wu, B.; Liu, Y.; Li, X.; Mamontov, E.; Kolesnikov, A. I.; Diallo, S. O.; Do, C.; Porcar, L.; Hong, K.; Smith, S. C.; *et al.* Charge-Dependent Dynamics of a Polyelectrolyte Dendrimer and Its Correlation with Invasive Water. *J. Am. Chem. Soc.* **2013**, *135*, 5111–5117.

(27) Liu, Y.; Porcar, L.; Hong, K.; Shew, C.-Y.; Li, X.; Liu, E.; Butler, P. D.; Herwig, K. W.; Smith, G. S.; Chen, W.-R. Effect of Counterion Valence on the pH Responsiveness of Polyamidoamine Dendrimer Structure. *J. Chem. Phys.* **2010**, *132*, 124901.

(28) Maingi, V.; Kumar, M. V. S.; Maiti, P. K. PAMAM Dendrimer-Drug Interactions: Effect of pH on the Binding and Release Pattern. *J. Phys. Chem. B* **2012**, *116*, 4370–4376.

(29) Lin, S.-T.; Maiti, P. K.; Goddard, W. A. Dynamics and Thermodynamics of Water in PAMAM Dendrimers at Subnanosecond Time Scales. *J. Phys. Chem. B* **2005**, *109*, 8663–8672.

(30) Maiti, P. K.; Bagchi, B. Diffusion of Flexible, Charged, Nanoscopic Molecules in Solution: Size and pH Dependence for PAMAM Dendrimer. *J. Chem. Phys.* **2009**, *131*, 214901.

(31) Ding, F.; Tsao, D.; Nie, H.; Dokholyan, N. V. Ab Initio Folding of Proteins with All-Atom Discrete Molecular Dynamics. *Structure* **2008**, *16*, 1010–1018.

(32) Yin, S.; Biedermannova, L.; Vondrasek, J.; Dokholyan, N. V. MedusaScore: An Accurate Force Field-Based Scoring Function for Virtual Drug Screening. *J. Chem. Inf. Model.* **2008**, *48*, 1656–1662.

(33) Ding, F.; Dokholyan, N. V. Emergence of Protein Fold Families through Rational Design. *PLoS Comput. Biol.* **2006**, *2*, e85.

(34) Andersen, H. C. Molecular Dynamics Simulations at Constant Pressure And/or Temperature. *J. Chem. Phys.* **1980**, *72*, 2384.

(35) Antosiewicz, J. M.; Shugar, D. Poisson-Boltzmann Continuum-Solvation Models: Applications to pH-Dependent Properties of Biomolecules. *Mol. Biosyst.* **2011**, *7*, 2923–2949.

(36) Porcar, L.; Liu, Y.; Verduzco, R.; Hong, K.; Paul, D.; Magid, L. J.; Smith, G. S.; Chen, W.; Butler, P. D. Structural Investigation of PAMAM Dendrimers in Aqueous Solutions Using Small-Angle Neutron Scattering : Effect of Generation Structural Investigation of PAMAM Dendrimers in Aqueous Solutions Using Small-Angle Neutron Scattering : Effect of Generation. *J. Phys. Chem. B* **2008**, *112*, 14772–14778.

(37) Porcar, L.; Hong, K.; Butler, P. D.; Herwig, K. W.; Smith, G. S.; Liu, Y.; Chen, W. Intramolecular Structural Change of PAMAM Dendrimers in Aqueous Solutions Revealed by Small-Angle Neutron Scattering. *J. Phys. Chem. B* **2010**, *114*, 1751–1756.

(38) Liu, Y.; Chen, C.-Y.; Chen, H.-L.; Hong, K.; Shew, C.-Y.; Li, X.; Liu, L.; Melnichenko, Y. B.; Smith, G. S.; Herwig, K. W.; *et al.* Electrostatic Swelling and Conformational Variation Observed in High-Generation Polyelectrolyte Dendrimers. *J. Phys. Chem. Lett.* **2010**, *1*, 2020–2024.

(39) Liu, Y.; Bryantsev, V. S.; Diallo, M. S.; Goddard, W. A. PAMAM Dendrimers Undergo pH Responsive Conformational Changes without Swelling. *J. Am. Chem. Soc.* **2009**, *131*, 2798–2799.

(40) Lee, H.; Larson, R. G. Molecular Dynamics Simulations of PAMAM Dendrimer-Induced Pore Formation in DPPC Bilayers with a Coarse-Grained Model. *J. Phys. Chem. B* **2006**, *110*, 18204–18211.

(41) Yang, L.; da Rocha, S. R. P. PEGylated, NH2-Terminated PAMAM Dendrimers: A Microscopic View from Atomistic Computer Simulations. *Mol. Pharm.* **2014**, *11*, 1459–1470.

(42) Niu, S.; Turro, C.; Bossmann, S. H.; Tomalia, D. A.; Turro, N. J. Binding of *Ru(phen)32+ to Starburst Dendrimers and Its Quenching by Co(phen)33+: Generation Dependence of the Quenching Rate Constant. *J. Phys. Chem.* **1995**, *99*, 5512–5517.

Table 1: Characterization of PAMAM Dendrimers[a]

Functionality	D_H (nm)	ζ (mV)
NH_2	4 ± 1	30.7 ± 2.9
OH	3 ± 1	-0.9 ± 1.0
SA	4 ± 1	-18.5 ± 2.0

a) D_H: Hydrodynamic diameter. ζ:Zeta Potential

Table 2: Comparison of R_g in PAMAM dendrimers from various works

	R_g (Å)		
	G3	G4	G5
Liu et al. - SANS[38]	16.7 ± 1.2	21.4 ± 0.4	26.8 ± 0.4
Lee & Larson- CG[40]	13.1 ± 0.1	---	23.2 ± 0.1
Liu et al. - MD[39]	15.8 ± 0.3	20.6 ± 0.2	25.3 ± 0.1
Yang & da Rocha – MD	15.0 ± 0.9	21.8 ± 0.8	23.8 ± 0.2
This Work (300 K)	15.7 ± 0.6	20.2 ± 0.6	25.7 ± 0.4

Figures

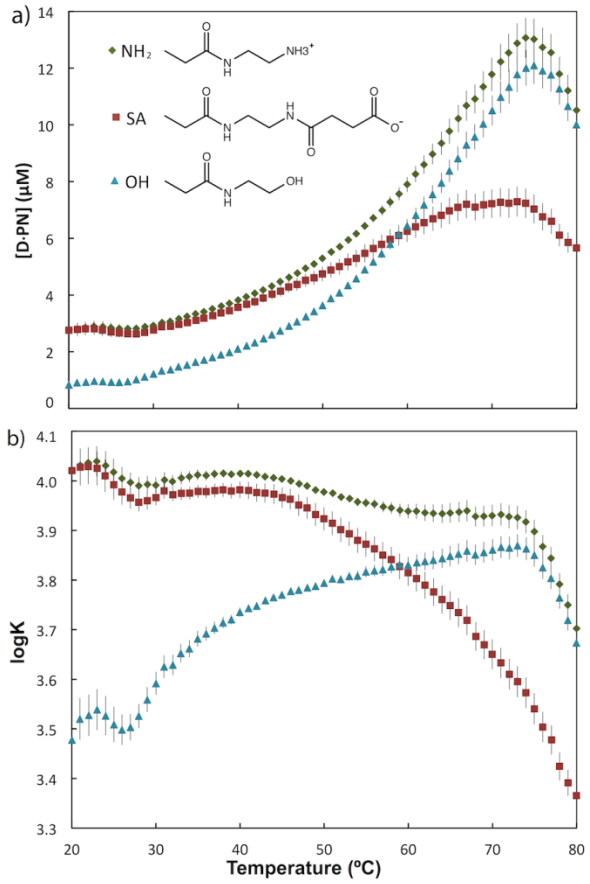

Figure 1. The concentration of dendrimer-associated phenanthrene (a) and the corresponding logK association constants (b) for G4-NH_2 (green diamonds), G4-SA (red squares), and G4-OH (blue triangles). Error bars are standard deviations of 3 independent trials. Note clear transition temperatures at 74°C where binding with phenanthrene becomes much less efficient. The inset in (a) shows the chemical structures of a single terminal chain of G4- NH_2, -SA, and -OH from top to bottom.

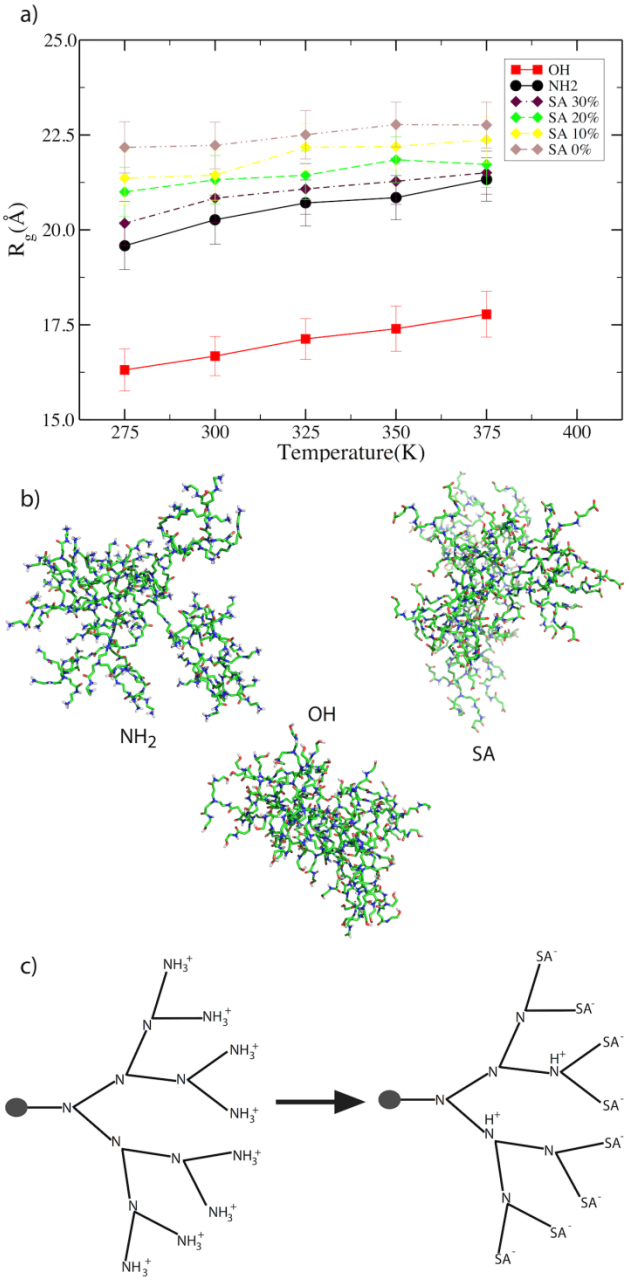

Figure 2. Radius of gyration (R_g) for G4-NH_2, OH, and SA for SA tertiary amine protonation fractions of 0-30% (a). Error bars are standard deviations taken across the 800 snapshots used in R_g calculations. Representative DMD snapshots of G4 PAMAM dendrimers at room temperature (b), which illustrates the effect of changing terminal group chemistry on the overall structure of the dendrimer. Differences in structure between G4-NH_2 and G4-SA are due to partial protonation of SA tertiary amines (c), with a portion of the dendrimer structure shown schematically emanating from a central core.

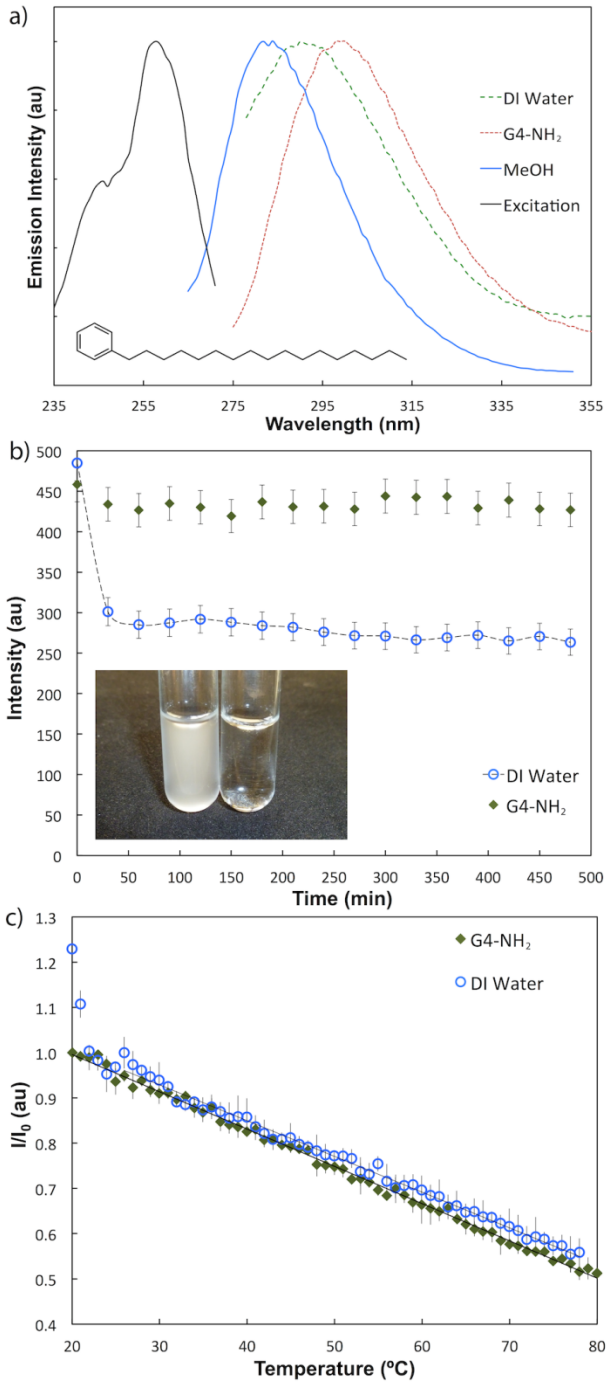

Figure 3. The fluorescence excitation and emission spectra (a) of ODB and the kinetics of this fluorescence at room temperature (b). Inset is a photo of pure water and dendrimer solutions incubated with equal quantities of C_{16}+ODB. Oil-in-water emulsions are cloudy suspensions (left); dispersion by dendrimers results in a clear suspension (right). Raising the solution temperature causes thermal quenching with and without dendrimers (c), but no loss of binding to dendrimers at high temperatures. Error bars are standard deviations of 3 independent trials.

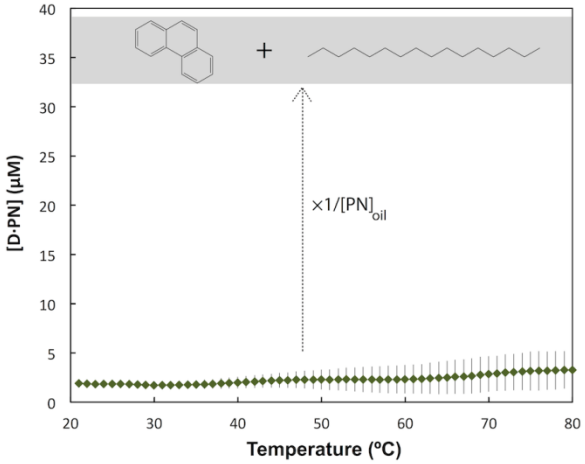

Figure 4. The concentration of dendrimer-associated PN (green diamonds) as a function of temperature. Shaded region shows the calculated increase in concentration of hydrocarbons due to dendrimers compared to oil-in water emulsion, including both PN and C_{16}. Error bars are standard deviations of 3 independent trials.

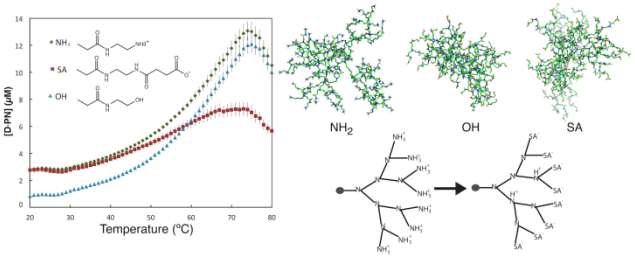

TOC Image